Biochimica et Biophysica Acta, 382 (1975) 125–141

BBA 76878

ESR SPECTRAL ANALYSIS OF THE MOLECULAR MOTION OF SPIN LABELS IN LIPID BILAYERS AND MEMBRANES BASED ON A MODEL IN TERMS OF TWO ANGULAR MOTIONAL PARAMETERS AND ROTATIONAL CORRELATION TIMES

JACOB ISRAELACHVILI, JAN SJÖSTEN, L. E. GÖRAN ERIKSSON, MAGDALENA EHRSTRÖM, ASTRID GRÄSLUND and ANDERS EHRENBERG*

Department of Biophysics, Stockholm University, Arrhenius Laboratory, S-104 05 Stockholm, Sweden

(Received August 22nd, 1974)

SUMMARY

Electron spin resonance (ESR) spectral line shapes are calculated for a nitroxide spin-labeled molecule undergoing rapid restricted rotations (twisting) about its long molecular axis while simultaneously tumbling within a cone. Explicit expressions are derived for the hyperfine splittings and g-values, as well as for the secular contributions to the motionally modulated linewidths. The present model is useful for analyzing the restricted twisting and tumbling motions, and rotational correlation times, of spin-labeled molecules in bilayers. Simulated spectra compare well with experimental spectra of lecithin bilayers marked with cholestane spin label, over a wide temperature range.

INTRODUCTION

The use of nitroxide spin-labeled fatty acids and steroids such as *I*(m,n) and *II* (Fig. 1) as probes of the local fluidity and structure of lipid bilayers and biological membranes is very wide-spread. However, it is only recently that physically realistic mathematical models have been invoked which satisfactorily describe the motion of these spin labels in bilayers and membranes. We have recently explored and applied one such model [1]. These models may be classified into two types depending on the approach: in one the spin labels are considered as undergoing diffusional rotations [2–4], while in the other their motion is assumed to be rapid but restricted or constrained within certain angular limits [1, 5–9]. The restricted motion models have assumed only one mode of motion, and have not shown explicitly how the linewidths of the three ESR lines depend on the motional parameters. Consequently, it has not been possible to accurately simulate ESR spectra using linewidth parameters directly related to the motional parameters (e.g. restricted angular limits of the motion,

* All correspondence should be addressed to Professor A. Ehrenberg.

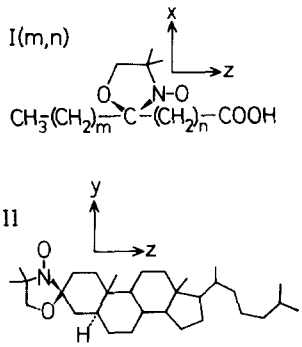

Fig. 1. Spin labels discussed in this paper. Note that in the present notation the axes x, y and z refer to the molecular axes of the molecule to which the nitroxide radical is attached, and not to the nitroxide radical principal axes. In spin label *I*(*m*, *n*) the oxazolidine ring lies in the x–y plane, while in spin label *II* it lies in the x–z plane. For spin label *II* the equatorial configuration of the nitrogen depicted above has been established [17].

correlation times, etc.). The present model assumes that the spin-labeled molecules are undergoing rapid restricted rotations (twisting) about their long molecular axes while simultaneously tumbling (wobbling) rapidly within the confines of a cone. The results for the effective g-values, hyperfine splittings, and the secular contributions to the motionally modulated linewidths of the three ESR lines are given in a form that allows for easy spectral simulation. This model is particularly useful for interpreting the ESR spectra of steroid spin labels such as *II* (Fig. 1); and computer-simulated spectra are found to compare well with experimental spectra of this spin label in randomly oriented lecithin bilayers.

THEORETICAL BASIS

The three ESR lines of a nitroxide radical attached to a tumbling molecule have eigenenergies given by (cf. ref. 1, but note differences in the coordinate axes systems applied)

$$E_0 = \beta_e \boldsymbol{H}_Z \langle g_{ZZ} \rangle = \beta_e \boldsymbol{H}_Z g'$$
$$E_{\pm 1} = E_0 \pm (\langle T_{XZ} \rangle^2 + \langle T_{YZ} \rangle^2 + \langle T_{ZZ} \rangle^2)^{\frac{1}{2}} = E_0 \pm T' \tag{1}$$

where

$$\begin{aligned} T_{XZ} &= (T_{xx} - T_{yy}) \sin\theta \sin\phi (\cos\theta \sin\phi \cos\psi + \cos\phi \sin\psi) \\ &\quad + (T_{zz} - T_{xx}) \sin\theta \cos\theta \cos\psi \\ T_{YZ} &= -(T_{xx} - T_{yy}) \sin\theta \sin\phi (\cos\theta \sin\phi \sin\psi - \cos\phi \cos\psi) \\ &\quad - (T_{zz} - T_{xx}) \sin\theta \cos\theta \sin\psi \\ T_{ZZ} &= T_{xx} \sin^2\theta \cos^2\phi + T_{yy} \sin^2\theta \sin^2\phi + T_{zz} \cos^2\theta \\ g_{ZZ} &= g_{xx} \sin^2\theta \cos^2\phi + g_{yy} \sin^2\theta \sin^2\phi + g_{zz} \cos^2\theta \end{aligned} \tag{2}$$

β_e is the Bohr magneton; $\boldsymbol{H}_Z$ is the external magnetic field which also defines the Z-axis of the laboratory XYZ coordinate system; g_{xx}, g_{yy}, g_{zz}, T_{xx}, T_{yy}, T_{zz} are the components of the diagonal g-value and hyperfine tensors of the radical along the

molecular axes xyz, which are related to the laboratory axes XYZ by the three Eulerian angles θ, ϕ and ψ. $\langle\ \rangle$ indicates partial or complete averaging over the angles θ, ϕ and ψ; and g' and T' may be thought of as the effective values of g and T. In the present notation g_{xx}, T_{xx}, etc. refer to the molecular axes (over which the averaging of the angles θ, ϕ and ψ is to be performed) and not the nitroxide radical axes. However, the axes of these two coordinate systems are assumed to be co-parallel (their z-axes may or may not coincide).

RAPID MOTION WITHIN A CONE MODEL

We shall adopt a model in which the molecular motion is determined by two independent angular variables ϕ_0 and β_0 as follows:

(1) *Axial rotations*: in which the molecule is rotating or twisting rapidly about its own z-axis (the long molecular axis of a steroid molecule) within an angular segment of amplitude $\pm\phi_0$, i.e. ϕ is averaged between $\phi'+\phi_0$ and $\phi'-\phi_0$.

(2) *Tumbling within a cone*: in which the molecular z-axis is tumbling rapidly within the confines of a cone of semi-cone angle β_0, where the cone axis subtends a fixed angle γ to the external field (Z-axis).

While ϕ_0 and β_0 are independent angular variables in this model, the two modes of motion within the cone are not independent but must be related through a physically realistic model. We shall adopt a model, shown in Fig. 2, in which the angle χ between the plane containing the instantaneous molecular z-axis and the cone axis and that containing the z-axis and the mean x-axis is independent of β. In Fig. 3 the external field (Z-axis) direction has been added, and the following relevant trigonometrical relations between the various angles are obtained (see also ref. 1, Fig. 1):

$$\cos\theta = \cos\gamma\cos\beta - \sin\gamma\sin\beta\cos\alpha \tag{3}$$

$$\sin^2\theta\cos 2\phi' = \{(\cos\gamma\sin\beta+\sin\gamma\cos\beta\cos\alpha)^2-(\sin\gamma\sin\alpha)^2\}\cos 2(\alpha-\eta) + 2(\cos\gamma\sin\beta+\sin\gamma\cos\beta\cos\alpha)(\sin\gamma\sin\alpha)\sin 2(\alpha-\eta) \tag{4}$$

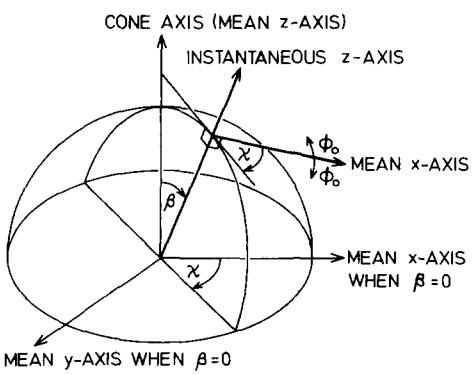

Fig. 2. In the present model the molecule is assumed to rotate or twist rapidly about its molecular z-axis with an angular amplitude $\pm\phi_0$, while at the same time tumbling rapidly within a cone of semicone angle β_0. The figure shows the instantaneous orientation of the molecule relative to the cone axis, where it is assumed that β and χ are independent.

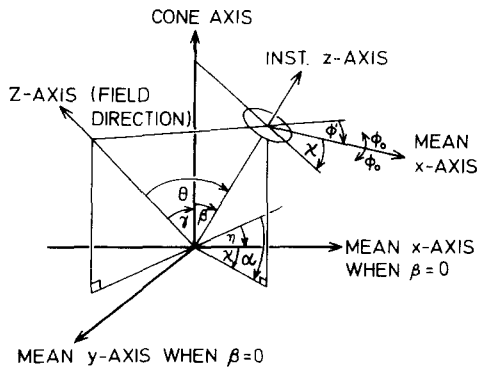

Fig. 3. The previous figure with the external field direction (Z-axis) added. γ is the angle between the fixed cone axis and the external field direction; β is the instantaneous angle between the molecular z-axis and the cone axis; θ is the instantaneous Eulerian angle θ between the molecular z-axis and the external field direction; ϕ' is the mean angle between the x–z and z–Z planes (i.e. ϕ' is the instantaneous Eulerian angle ϕ referred to the mean molecular x-axis), and η is the value of ϕ' when $\beta = 0$; χ is an arbitrary angle such that $\chi = \alpha - \eta$. The Eulerian angle ψ is not shown (see ref. 1, Fig. 1). By use of the cosine theorem it may be shown that $\cos(\chi + \phi') = \cos(\alpha - \eta + \phi') = (\cos\gamma' \sin\beta - \sin\gamma' \cos\beta \cos\alpha)/\sin\theta$, and by use of Eqn 3 we arrive at Eqn 4. The averaging over θ, ψ and ϕ is effected by allowing ϕ to take on all values between $\phi' - \phi_0$ and $\phi' + \phi_0$, then allowing α and β to take on all values between 0 and 2π, and 0 and β_0, respectively.

$$\sin(\psi_0 - \psi) = \sin\beta \sin\alpha/\sin\theta \tag{5}$$

We shall first deal with the secular contributions to g' and T', given by $\langle g_{ZZ} \rangle$ and $\langle T_{ZZ} \rangle$, the evaluation of which involves calculating the averages $\langle \cos^2\theta \rangle$, $\langle \sin^2\theta \cos^2\phi \rangle$ and $\langle \sin^2\theta \sin^2\phi \rangle$ as follows (with Eqn 3):

$$1.\quad \langle \cos^2\theta \rangle = 1 - \langle \sin^2\theta \rangle = \frac{\int_0^{2\pi} d\alpha \int_0^{\beta_0} \cos^2\theta \sin\beta \cdot d\beta}{\int_0^{2\pi} d\alpha \int_0^{\beta_0} \sin\beta \cdot d\beta}$$

$$= \tfrac{1}{6}\{2 + (3\cos^2\gamma - 1)(1 + \cos\beta_0)\cos\beta_0\} \tag{6}$$

$$2.\quad \langle \sin^2\theta \cos^2\phi \rangle = \frac{\int_0^{2\pi} d\alpha \int_0^{\beta_0} \sin^2\theta \sin\beta \cdot d\beta \int_{\phi'-\phi_0}^{\phi'+\phi_0} \cos^2\phi \, d\phi}{\int_0^{2\pi} d\alpha \int_0^{\beta_0} \sin\beta \cdot d\beta \int_{\phi'-\phi_0}^{\phi'+\phi_0} d\phi}$$

$$= \frac{\int_0^{2\pi} d\alpha \int_0^{\beta_0} \sin^2\theta \cdot \sin\beta \cdot d\beta \cdot \tfrac{1}{2}\left[1 + \dfrac{\sin\phi_0 \cos\phi_0}{\phi_0} \cos 2\phi'\right]}{2\pi(1 - \cos\beta_0)}$$

$$\text{(with Eqn 4)} \qquad = \tfrac{1}{2}\langle \sin^2\theta \rangle + \sigma \cdot \frac{\sin^2\gamma \cos 2\eta}{24}(7 + 4\cos\beta_0 + \cos^2\beta_0) \tag{7}$$

$$3.\quad \langle \sin^2\theta \sin^2\phi\rangle = \tfrac{1}{2}\langle \sin^2\theta\rangle - \sigma \cdot \frac{\sin^2\gamma \cos 2\eta}{24}(7+4\cos\beta_0+\cos^2\beta_0) \tag{8}$$

$$\text{where } \sigma = \frac{\sin\phi_0 \cos\phi_0}{\phi_0} \tag{9}$$

Substituting Eqns 6–8 into the expression for the effective g-value

$$g' = \langle g_{ZZ}\rangle = g_{xx}\langle \sin^2\theta\cos^2\phi\rangle + g_{yy}\langle \sin^2\theta \sin^2\phi\rangle + g_{zz}\langle \cos^2\theta\rangle \tag{10}$$

we obtain an expression for g' which may be put in the convenient form

$$g' = \bar{g}_{xx}\sin^2\gamma\cos^2\eta + \bar{g}_{yy}\sin^2\gamma\sin^2\eta + \bar{g}_{zz}\cos^2\gamma \tag{11a}$$

where

$$\bar{g}_{xx} = \tfrac{1}{2}\left[(g_{xx}+g_{yy})-(g_{yy}-g_{xx})\,\sigma\left(\frac{7+4\cos\beta_0+\cos^2\beta_0}{12}\right)\right] + [g_{zz}-\tfrac{1}{2}(g_{xx}+g_{yy})]\left(\frac{2-\cos\beta_0-\cos^2\beta_0}{6}\right) \tag{11b}$$

$$\bar{g}_{yy} = \tfrac{1}{2}\left[(g_{xx}+g_{yy})+(g_{yy}-g_{xx})\,\sigma\left(\frac{7+4\cos\beta_0+\cos^2\beta_0}{12}\right)\right] + [g_{zz}-\tfrac{1}{2}(g_{xx}+g_{yy})]\left(\frac{2-\cos\beta_0-\cos^2\beta_0}{6}\right) \tag{11c}$$

$$\bar{g}_{zz} = \tfrac{1}{2}(g_{xx}+g_{yy})+[g_{zz}-\tfrac{1}{2}(g_{xx}+g_{yy})]\left(\frac{1+\cos\beta_0+\cos^2\beta_0}{3}\right) \tag{11d}$$

Note that $\bar{g}_{xx}+\bar{g}_{yy}+\bar{g}_{zz} = g_{xx}+g_{yy}+g_{zz}$.

The expression for $\langle T_{ZZ}\rangle$ has the same form as Eqn 11 with g_{xx}, $\bar{g}_{xx}$, g_{yy}, etc. replaced by T_{xx}, $\overline{T}_{xx}$, T_{yy}, etc.

In order to calculate T', many pseudosecular terms have also to be averaged (see Eqns 1 and 2 and the resulting computations are very tedious. However, it is reasonable to expect that T' takes the form

$$T' = (\overline{T}_{xx}^2\sin^2\gamma\cos^2\eta + \overline{T}_{yy}^2\sin^2\gamma\sin^2\eta + \overline{T}_{zz}^2\cos^2\gamma)^{\frac{1}{2}} \tag{12a}$$

whence we may calculate $\overline{T}_{xx}$, $\overline{T}_{yy}$ and $\overline{T}_{zz}$ on the basis of the present model (putting $\gamma = 90°$, $\eta = 0$; $\gamma = 90°$, $\eta = 90°$; $\gamma = 0°$, respectively. into Eqns 3, 4 and 5). In these limits it may be shown that the pseudosecular terms of Eqn 2 do not contribute to the hyperfine splittings and we therefore obtain

$$\overline{T}_{xx} = \tfrac{1}{2}\left[(T_{xx}+T_{yy})-(T_{yy}-T_{xx})\,\sigma\left(\frac{7+4\cos\beta_0+\cos^2\beta_0}{12}\right)\right] + [T_{zz}-\tfrac{1}{2}(T_{xx}+T_{yy})]\left(\frac{2-\cos\beta_0-\cos^2\beta_0}{6}\right) \tag{12b}$$

$$\bar{T}_{xx} = \tfrac{1}{2}\left[(T_{xx}+T_{yy})+(T_{xx}-T_{yy})\sigma\left(\frac{7+4\cos\beta_0+\cos^2\beta_0}{12}\right)\right]$$
$$+ [T_{zz}-\tfrac{1}{2}(T_{xx}+T_{yy})]\left(\frac{2-\cos\beta_0-\cos^2\beta_0}{6}\right) \quad (12c)$$

$$\bar{T}_{zz} = \tfrac{1}{2}(T_{xx}+T_{yy})+[T_{zz}-\tfrac{1}{2}(T_{xx}+T_{yy})]\left(\frac{1+\cos\beta_0+\cos^2\beta_0}{3}\right) \quad (12d)$$

and $\bar{T}_{xx}+\bar{T}_{yy}+\bar{T}_{zz} = T_{xx}+T_{yy}+T_{zz}$.

Though Eqn 12 has not been derived rigorously it nevertheless reduces to the correct expressions in all the limiting cases where a comparison with existing rigorously derived expressions can be made.

Eqns 11 and 12 have the following limiting forms:

1. For no motion ($\phi_0 = 0$, $\beta_0 = 0$, so that $\sigma = 1$, $\gamma = 0$, $\eta = \phi$)

$$\bar{g}_{xx} = g_{xx}, \bar{g}_{yy} = g_{yy}, \bar{g}_{zz} = g_{zz},$$

and similarly for $\bar{T}_{xx}$, etc.

2. For complete isotropic motion ($\phi_0 = 90°$, $\beta_0 = 90°$, so that $\sigma = 0$)

$$\bar{g}_{xx} = \bar{g}_{yy} = \bar{g}_{zz} = \tfrac{1}{3}(g_{xx}+g_{yy}+g_{zz}),$$

and similarly for $\bar{T}_{xx}$, etc.

3. For no tumbling within a cone ($\beta_0 = 0$)

$$\bar{g}_{xx} = \tfrac{1}{2}[(g_{xx}+g_{yy})-(g_{yy}-g_{xx})\sigma]$$
$$\bar{g}_{yy} = \tfrac{1}{2}[(g_{xx}+g_{yy})+(g_{yy}-g_{xx})\sigma]$$
$$\bar{g}_{zz} = g_{zz}$$

and similarly, for $\bar{T}_{xx}$, etc. Eqns 11 and 12 reduce to results recently derived by Jost and Griffith [8] for this case (though their notation for the xyz axes differs from ours).

4. For complete axial rotations ($\phi_0 = 90°$, $\sigma = 0$)

$$\bar{g}_{xx} = \bar{g}_{yy} = \tfrac{1}{2}(g_{xx}+g_{yy})+[g_{zz}-\tfrac{1}{2}(g_{xx}+g_{yy})]\left(\frac{2-\cos\beta_0-\cos^2\beta_0}{6}\right)$$

$$\bar{g}_{zz} = \tfrac{1}{2}(g_{xx}+g_{yy})+[g_{zz}-\tfrac{1}{2}(g_{xx}+g_{yy})]\left(\frac{1+\cos\beta_0+\cos^2\beta_0}{3}\right)$$

Eqns 11 and 12 are now equivalent to expressions recently derived by Israelachvili et al. (ref. 1, Eqns 13 and 16) for this case, where pseudosecular terms were included in the averaging over all angles.

The factor σ serves as a useful measure of the rotational motion of the molecule about its own z-axis. The twisting angle ϕ_0 appears in Eqns 11 and 12 only in the form σ; and we may further note that, when $\beta_0 = 0$,

$$\sigma = \frac{\bar{T}_{xx}-\bar{T}_{yy}}{T_{xx}-T_{yy}} = \frac{\sin\phi_0\cos\phi_0}{\phi_0} \quad (13)$$

The factor σ may be referred to as the axial order (motional) parameter. For no axial rotations $\sigma = 1$, while for complete axial rotations $\sigma = 0$.

Note that σ is independent of the conventional order parameter

$$S = \frac{\overline{T}_{zz} - \frac{1}{2}(\overline{T}_{xx} + \overline{T}_{yy})}{T_{zz} - \frac{1}{2}(T_{xx} + T_{yy})} = \tfrac{1}{2}\cos\beta_0(1+\cos\beta_0) \tag{14}$$

which defines the tumbling motion within the cone and which varies between 1 and 0 as β_0 varies between 0 (no motion) and 90° (rapid tumbling). The two order parameters S and σ therefore serve to define the two modes of motion of the molecule in the present model.

On the basis of the present model ESR spectral line shapes will depend on both ϕ_0 and β_0, as well as on the spatial distribution of cone axis inclinations γ. If there is a random distribution of cone axes then simulated spectra can be obtained by employing the standard programme of Lefebvre and Maruani [10] with the Eulerian angles θ and ϕ now replaced by γ and η, and using values for $\overline{T}_{xx}$, $\overline{g}_{xx}$, etc. as calculated from Eqns 11 and 12. Thus, if $\overline{T}_{xx}$, $\overline{T}_{yy}$, $\overline{T}_{zz}$ can be determined from a best-fit spectral simulation of an experimental spectrum, one immediately obtains unique values for ϕ_0 and β_0. Good simulations, however, are rarely obtained without some linewidth consideration (the Lefebvre and Maruani programme assumes a constant intrinsic linewidth for all the lines), and this matter will now be dealt with.

LINEWIDTH CONTRIBUTIONS FROM MOTIONAL MODULATION

The rotational motion of a nitroxide radical results in a "modulation" broadening of each ESR line. This broadening depends on the anisotropic g and T tensor components, on the nuclear spin quantum number m, and, in the present model, on the motional parameters γ, β_0, η, ϕ_0, and on the rotational correlation time τ.

For rapid interchanges in orientation, as is assumed in the present model, the linewidth contribution from motional modulation is proportional to the mean square fluctuation of the instantaneous resonant field about the mean [11, 12]. The total linewidth may therefore be expressed as

$$\Gamma_m = \Gamma_r + \langle (H - \langle H \rangle)^2 \rangle \gamma_e \tau \tag{15}$$

where Γ_m is the half-width at half-height of the absorption line*; Γ_r is the residual linewidth, assumed the same for all lines; H is the instantaneous resonant field at the fixed microwave frequency ν; γ_e is the magnetogyric ratio of a free electron, and τ is the rotational correlation time of the tumbling molecule. The motional narrowing situation of Eqn 15 is valid when the time-dependent fluctuation $\delta H = H - \langle H \rangle$ obeys $\langle \delta H \rangle^2 \gamma_e{}^2 \tau^2 < 1$ [12]. For a nitroxide spin label the maximal value of $\langle \delta H \rangle$ $\gamma_e \approx 5 \cdot 10^8$ rad/s from the hyperfine contribution. For isotropic motion the theory is thus applicable for $\tau \leqslant 2 \cdot 10^{-9}$ s. For restricted anisotropic motion (small β_0 and ϕ_0) the fluctuation δH decreases and hence the theory will be valid for correspondingly larger τ-values. In the present analysis we shall concentrate only on the secular contribution to the linewidth. For simplicity we neglect the non-secular effects and assume $(2\pi\nu)\,\tau > 1$, where ν is the resonance frequency ($\tau > 2 \cdot 10^{-11}$ s at X-band).

* If W is the peak derivative width, then $W = (2/\sqrt{3})\Gamma$ for a Lorentzian line, and $W = (2/\ln 2)^{\frac{1}{2}}\,\Gamma$ for a Gaussian line.

Putting:

$$\begin{aligned}
\Delta T &= T_{zz} - \tfrac{1}{2}(T_{xx} + T_{yy}) \\
\delta T &= T_{xx} - T_{yy} \\
T_0 &= \tfrac{1}{3}(T_{xx} + T_{yy} + T_{zz}) \\
\Delta g &= g_{zz} - \tfrac{1}{2}(g_{xx} + g_{yy}) \\
\delta g &= g_{xx} - g_{yy} \\
g_0 &= \tfrac{1}{3}(g_{xx} + g_{yy} + g_{zz})
\end{aligned} \tag{16}$$

we may express g_{ZZ} of Eqn 2 in the form

$$g_{ZZ} = g_0 + \tfrac{1}{3}\Delta g(3\cos^2\theta - 1) + \tfrac{1}{2}\delta g \sin^2\theta \cos 2\phi, \tag{17}$$

and similarly for T_{ZZ}.

Thus:

$$\begin{aligned}
H &\approx \frac{h\nu}{\beta_e g_{ZZ}} - \mathrm{m}T_{ZZ} \\
&\approx \frac{h\nu}{\beta_e g_0^2}\left[g_0 - \{\tfrac{1}{3}\Delta g(3\cos^2\theta - 1) + \tfrac{1}{2}\delta g \sin^2\theta \cos 2\phi\}\right] \\
&\quad - \mathrm{m}\left[T_0 + \{\tfrac{1}{3}\Delta T(3\cos^2\theta - 1) + \tfrac{1}{2}\delta T \sin^2\theta \cos 2\phi\}\right] \\
&= \mathrm{CONST} - \left(\frac{h\nu}{\beta_e g_0^2}\Delta g + \mathrm{m}\Delta T\right)\cos^2\theta - \frac{1}{2}\left(\frac{h\nu}{\beta_e g_0^2}\delta g + \mathrm{m}\delta T\right)\sin^2\theta \cos 2\phi
\end{aligned} \tag{18}$$

Hence:

$$\begin{aligned}
\Gamma_m = \Gamma_r + \Bigg[&\left(\frac{h\nu}{\beta_e g_0^2}\Delta g + \mathrm{m}\Delta T\right)^2(\langle\cos^4\theta\rangle - \langle\cos^2\theta\rangle^2) \\
&+ \left(\frac{h\nu}{\beta_e g_0^2}\Delta g + \mathrm{m}\Delta T\right)\left(\frac{h\nu}{\beta_e g_0^2}\delta g + \mathrm{m}\delta T\right)(\langle\sin^2\theta\cos^2\theta\cos 2\phi\rangle \\
&\qquad - \langle\cos^2\theta\rangle\langle\sin^2\theta\cos 2\phi\rangle) \\
&+ \frac{1}{4}\left(\frac{h\nu}{\beta_e g_0^2}\delta g + \mathrm{m}\delta T\right)^2(\langle\sin^4\theta\cos^2 2\phi\rangle - \langle\sin^2\theta\cos 2\phi\rangle^2)\Bigg]\gamma_e\tau
\end{aligned} \tag{19}$$

In the limit of rapid isotropic tumbling (τ isotropic) the only nonvanishing terms are $\langle\cos^4\theta\rangle = \frac{1}{5}$, $\langle\cos^2\theta\rangle = \frac{1}{3}$, and $\langle\sin^4\theta\cos^2 2\phi\rangle = \frac{4}{15}$, and the linewidth is then:

$$\Gamma_m = \Gamma_r + \left[\frac{4}{45}\left(\frac{h\nu}{\beta_e g_0^2}\Delta g + \mathrm{m}\Delta T\right)^2 + \frac{1}{15}\left(\frac{h\nu}{\beta_e g_0^2}\delta g + \mathrm{m}\delta T\right)^2\right]\gamma_e\tau \tag{20}$$

Eqn 20 is in complete agreeement with Wilson and Kivelsons' results (ref. 13, Table III) regarding the secular contributions to the linewidth in the limit of rapid isotropic tumbling. Also in this limit, the pseudosecular contribution to the linewidth [13] is: $\frac{3}{8}(\frac{4}{45}\Delta T^2 + \frac{1}{15}\delta T^2)[I(I+1) - \mathrm{m}^2]\gamma_e\tau$.

In the case of restricted rotations each term of Eqn 19 must be averaged on the basis of the present (or some other) model. The general expression for Γ_m is very complicated. However, for steroid spin labels (e.g. *II*) it is sufficient to consider only the two limiting cases of $\phi_0 > 0$, $\beta_0 = 0$, and $\phi_0 = 90°$, $\beta_0 > 0$. This is because a steroid molecule in a bilayer does not tumble appreciably within a cone until the axial rotations are complete.

Case 1: *Axial rotations only* ($\phi_0 > 0$); *no motion within a cone* ($\beta_0 = 0$)

When $\beta_0 = 0$, $\theta = \gamma$, and $\phi' = \eta$; the first two terms within the square brackets in Eqn 19 vanish, and we are left with

$$\Gamma_m = \Gamma_r + \tfrac{1}{4}\left(\frac{h\nu}{\beta_e g_0^2}\delta g + m\delta T\right)^2 \sin^4\gamma[\langle\cos^2 2\phi\rangle - \langle\cos 2\phi\rangle^2]\gamma_e\tau_a$$

$$= \Gamma_r + \tfrac{1}{4}\left(\frac{h\nu}{\beta_e g_0^2}\delta g + m\delta T\right)^2 \sin^4\gamma[\tfrac{1}{2}(1-\sigma\cos 2\phi_0) - \sigma\cos^2 2\eta(\sigma - \cos 2\phi_0)]\gamma_e\tau_a \tag{21}$$

where τ_a is the axial rotational correlation time of the molecule (since Eqn 21 arises from pure axial rotations about the molecular z-axis). Fig. 4 shows how $\frac{1}{4}(\langle\cos^2 2\phi\rangle - \langle\cos 2\phi\rangle^2)$ varies with ϕ_0 and η.

For no axial rotations ($\phi_0 = 0$, $\sigma = 1$), $\Gamma_m = \Gamma_r$; while for complete axial rotations ($\sigma = 0$),

$$\Gamma_m = \Gamma_r + \tfrac{1}{8}\left(\frac{h\nu}{\beta_e g_0^2}\delta g + m\delta T\right)^2 (\sin^4\gamma)\gamma_e\tau_a \tag{22}$$

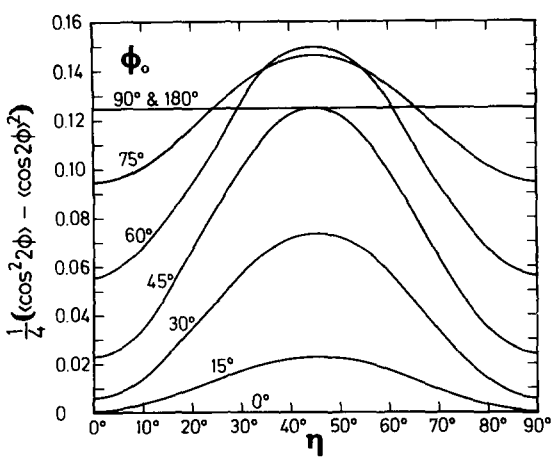

Fig. 4. Variation of $\frac{1}{4}(\langle\cos^2 2\phi\rangle - \langle\cos 2\phi\rangle^2)$ with angle η at different values of ϕ_0. For a nitroxide spin label attached to a steroid molecule such as cholestane (spin label *II*) that is rotating or twisting rapidly about its long molecular axis (the z-axis) within an angular segment of amplitude $\pm\phi_0$, the effective g and T values at a given inclination γ and η are given by Eqns 11 and 12 putting $\beta_0 = 0$, and the secular linewidths of the three ESR lines (at $m = 0, \pm 1$) are given by Eqn 21. The above linewidth variations are symmetrical about $\eta = 45°$, and show that the largest linewidth occurs at $\gamma = 90°$, $\eta = 45°$.

It may also be shown that in this limit the pseudosecular contribution to the linewidth is $\frac{1}{32}\delta T^2 \sin^2\gamma\,(1+\cos^2\gamma)\,(I(I+1)-m^2)\,\gamma_e\tau_a$.

Case 2: Complete axial rotations ($\phi_0 = 90°$), *plus motion within a cone* ($\beta_0 > 0$)

All terms in which $\cos 2\phi$ appears within $\langle\ \rangle$ brackets in Eqn 19 now vanish and we have

$$\Gamma_m = \Gamma_r + \left(\frac{h\nu}{\beta_e g_0^2}\Delta g + m\Delta T\right)^2 (\langle\cos^4\theta\rangle - \langle\cos^2\theta\rangle^2)\gamma_e\tau_t + \tfrac{1}{8}\left(\frac{h\nu}{\beta_e g_0^2}\delta g + m\delta T\right)^2 \langle\sin^4\theta\rangle\gamma_e\tau_{at} \qquad (23)$$

As the second term in Eqn 23 arises from pure tumbling within the cone, τ_t is the tumbling corelation time. The third term in Eqn 23 arises from both axial rotations and tumbling (cf. arguments on p. 127 and Figs 2 and 3), so that τ_{at} represents a mixed correlation time intermediate between τ_a and τ_t.

Using Eq (3) and averaging as before, we obtain

$$\begin{aligned}\langle\cos^4\theta\rangle - \langle\cos^2\theta\rangle^2 = {} & \tfrac{1}{45}(1-\cos\beta_0)^2(4+7\cos\beta_0+4\cos^2\beta_0) \\ & + \tfrac{1}{3}\sin^2\gamma\cos\beta_0(1+2\cos\beta_0)(1-\cos^2\beta_0) \\ & - \tfrac{1}{8}\sin^4\gamma\cos\beta_0(3+5\cos\beta_0)(1-\cos^2\beta_0) \end{aligned} \qquad (24)$$

and

$$\begin{aligned}\langle\sin^4\theta\rangle = {} & \tfrac{1}{15}(1-\cos\beta_0)^2(8+9\cos\beta_0+3\cos^2\beta_0) \\ & + \sin^2\gamma\cos\beta_0(1+\cos\beta_0)(1-\cos^2\beta_0) \\ & + \tfrac{1}{8}\sin^4\gamma\cos\beta_0(1+\cos\beta_0)(7\cos^2\beta_0-3) \end{aligned} \qquad (25)$$

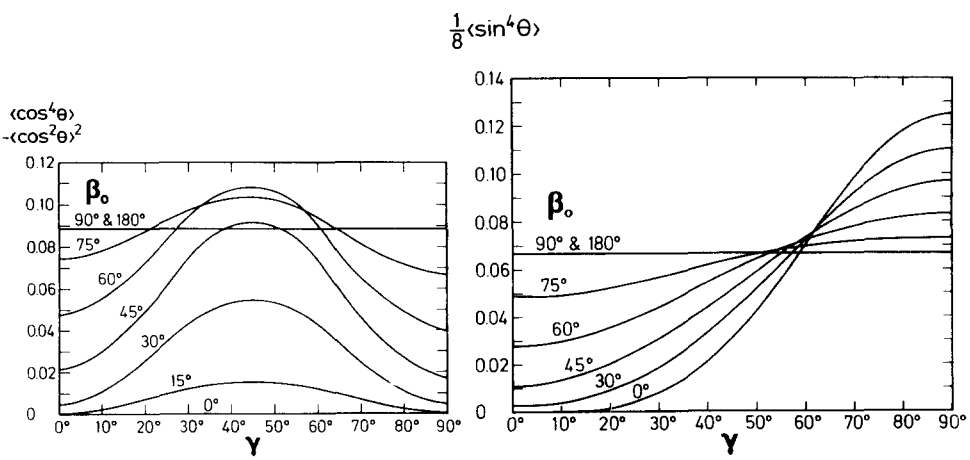

Fig. 5. (a) Variation of $\langle\cos^4\theta\rangle - \langle\cos^2\theta\rangle^2$ with angle γ at different values of β_0. (b) Variation of $\frac{1}{8}\langle\sin^4\theta\rangle$ with angle γ at different values of β_0. For a spin-labeled molecule which is rotating rapidly about its molecular z-axis, and at the same time tumbling within a cone of semi-cone angle β_0, the effective g and T values at a given cone axis inclination γ to the external field are given by Eqns 11 and 12 putting $\sigma = 0$, and the secular linewidths of the three ESR lines (at $m = 0, \pm 1$) are given by Eqn 23.

For no motion within a cone ($\beta_0 = 0$) Eqn 23 reduces to Eqn 22, while for rapid isotropic tumbling Eqn 23 reduces to Eqn 20. Fig. 5 shows how ($\langle\cos^4\theta\rangle - \langle\cos^2\theta\rangle^2$) and $\frac{1}{8}\langle\sin^4\theta\rangle$ vary with β_0 and γ.

For steroid spin labels such as *II*, Δg and ΔT, and δg and δT, have different signs, so that the high field ($m = -1$) lines will always be broader than the low field ($m = +1$) lines.

For spin labels such as fatty acids, $I(m, n)$, Δg and ΔT are also of different sign, while δT is now negligibly small. Hence for such spin labels the high field ($m = -1$) lines will again be broader than the low field ($m = +1$) lines, and the linewidth is satisfactory given by the first two terms of Eqn 23.

APPLICATION OF THE MODEL TO STEROID SPIN LABELS

For a steroid spin label such as *II*, there is a large difference between T_{xx} and T_{yy}, and the spectra are very sensitive to changes in both ϕ_0 and β_0 (as well as Γ_r and τ).

In order to obtain the best values for ϕ_0 and β_0 one must resort to best-fit computer simulations. This process is facilitated by the following two considerations: First, we may expect that a steroid molecule in a bilayer will first rotate about its own z-axis before tumbling within a cone. Thus, as the temperature is raised from a low value, where $\phi_0 = \beta_0 = 0$ corresponding to a powder spectrum, ϕ_0 should be the first to increase, and only when ϕ_0 is close to 90° should β_0 begin to rise above 0. Second, for cholestane spin label *II*, $T_{yy} > T_{xx} \approx T_{zz}$, so that the effective hyperfine splitting T' of Eqn 12a is maximum when $\gamma = 90°$, $\eta = 90°$, i.e.

$$T'_{max} = \overline{T}_{yy} \quad \text{(c.f. Eqn 12c)} \tag{26}$$

Thus, for no motion ($\sigma = 1$, $\beta_0 = 0$) $T'_{max} = T_{yy}$; for rapid axial rotations only ($\sigma = 0$, $\beta_0 = 0$) $T'_{max} = \frac{1}{2}(T_{xx}+T_{yy})$; while for rapid isotropic motion ($\sigma = 0$, $\beta_0 = 90°$) $T'_{max} = \frac{1}{3}(T_{xx}+T_{yy}+T_{zz})$.

T'_{max} is a useful parameter that may be obtained approximately from experimental spectra by measuring the field separation of the high and low field derivative extrema, $2T'_{max}$ (exp). Computer simulated spectra for the present model, however, reveal that the separation between the high and low field extrema, as measured from the simulated spectra, increases progressively above $2T'_{max}$ (the input value for the simulation) as τ increases. This is because the greatest linewidth broadening does not occur at the outermost spectral regions but farther in as may be seen from Figs 4 and 5 and the corresponding equations. The measured value of $2T'_{max}$ (exp), however, remains a useful starting parameter for simulations.

EXPERIMENTAL

Cholestane spin label (3-doxyl-5α-cholestane, Fig. 1), obtained from SYVA, Palo Alto, Calif.) and egg yolk lecithin (type IIIe, obtained from Sigma Chemical Co., and used without further purification) were dissolved in hexane in a molar ratio 1 : 100 The mixture was evaporated to dryness flask, A 0.1 M NaCl solution buffered with 50 mM Tris (pH 7.2) was added to the flask, which was then rotated slowly in a

waterbath at ~37 °C until the film containing the cholestane/lecithin mixture had dissolved (30–40 min). The solution was homogenized by sonicating for 10 minutes in a Branson S-125 sonicator at power level 4, and then centrifuged at 48 000 *g* for 10 min. The supernatant was collected and inserted into a quartz ESR capillary tube of 1 mm inner bore. The final concentration of lecithin was 15 mg/ml.

ESR spectra were recorded with a Varian E-9 X-band spectrometer using a rectangular cavity. The temperature was regulated with a heater/sensor system using cold nitrogen gas, and the sample temperature was measured with a platinum resistance (before and after each spectrum) to ±0.2 °C.

For accurate *g*-value and field calibrations of the "frozen" powder spectrum, at −196 °C, an AEG NMR field meter and a frequency counter (for both the microwave and NMR frequencies) were used.

Simulated ESR spectra were computed on an IBM 360/75 with a program that included variations of an arbitrary lineshape as a subroutine. The spectra could be scaled to the same maximum peak-to-peak amplitude, or normalized to an identical double integral.

RESULTS AND DISSCUSSION

Experimental spectra

Sonicated and unsonicated lecithin dispersions exhibited almost identical spectra at 22 °C. Fig. 6 (broken lines) shows a number of selected experimental spectra of the sonicated dispersion at different temperatures. The top spectrum (6a; at −31 °C) corresponds to a powder spectrum centred at $g = 2.0021$, and of maximum splitting

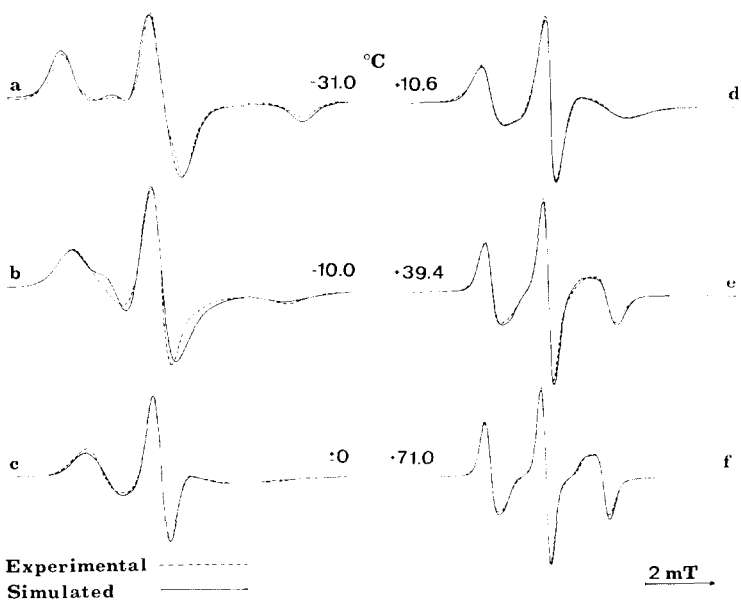

Fig. 6. Comparison between experimental (broken line) and stimulated (full line) ESR spectra at various temperatures for the 3-doxyl-cholestane spin label in aqueous egg lecithin dispersions. The parameter sets used for the simulation of the various spectra are found in Table I.

T'_{max} (exp) = 3.42 mT. At this temperature the spin labels are almost completely immobilized; on further lowering the temperature to −196 °C there was no further increase of the maximum splitting, but only a broadening of the spectrum.

The overall spectral line shapes were completely reversible in the temperature range studied (−31 °C to +71 °C), though the intensity of the signal fell by ~20% during the course of the measurements (~15 h).

Simulated spectra

Fig. 6 (continuous lines superimposed on the experimental broken lines) shows computer-simulated spectra based on the present model, each calculated at the best-fit values of ϕ_0, β_0, W_r, and τ, as shown in Table I.

TABLE I

PARAMETERS USED FOR SIMULATING THE ESR SPECTRA IN FIGS 6a–f

Temp. (°C)	ϕ_0 (degrees)	β_0 (degrees)	W_r* (mT)	τ_a (ns)	τ_t (ns)	τ_{at} (ns)
−31.8	6.0	0	0.62	10.0	—	—
−10.0	43.0	0	0.60	5.0	—	—
±0	66.0	0	0.42	3.0	—	—
+10.6	90.0	25.0	0.42	—	3.0	1.5
+39.4	90.0	52.0	0.35	—	2.0	0.3
+71.0	90.0	59.0	0.30	—	0.5	0.1

* A superposition of Gaussian and Lorentzian functions in an 1 : 1 ratio both with the indicated linewidths was employed.

Each spectrum was obtained by adding spectra at 2.5 ° intervals of η and γ from $\eta = 1.25°$ to $\eta = 88.75°$ and from $\gamma = 1.25°$ to $\gamma = 88.75°$, each weighted with $\sin\gamma$ (to account for the random distribution of γ and η in all directions). The functions $g'(\gamma, \beta_0, \eta, \phi_0)$, $T'(\gamma, \beta_0, \eta, \phi_0)$ were calculated using Eqns 11 and 12; and the linewidths Γ_m (and W_m*) of the three ESR lines ($m = 0, \pm 1$) per spectrum were calculated using Eqns 21 or 23, whichever was the more appropriate.

The following g and T values were used in the simulations:

$g_{xx} = 2.0083$ (best-fit)
$g_{yy} = 2.0021$ (measured)
$g_{zz} = 2.0064$ (best-fit)
$T_{xx} = 0.56$ mT (best-fit)
$T_{yy} = 3.42$ mT (measured)
$T_{zz} = 0.56$ mT (best-fit) and $\nu = 9.05 \times 10^9$ Hz (experimental microwave frequency).

Thus

$g_0 = 2.0056$ $\quad T_0 = 1.51$ mT
$(h\nu/\beta_e g_0^2)\Delta g = 0.19$ mT $\quad \Delta T = -1.43$ mT
$(h\nu/\beta_e g_0^2)\delta g = 1.00$ mT $\quad \delta T = -2.86$ mT

* See footnote p. 131.

To start with we used g_{xx} 2.0088 and g_{zz} 2.0058 according to the literature [6, 14]. These values, however, invariably caused a shift of the central zero-crossing towards high fields, hence small adjustments of the g-components were necessary, while keeping g_0 unchanged.

Using these values in Eqns 19–23, we readily find that the motional broadening of the three ESR lines is in the order: high field (m 1) low field (m 1) centre field (m 0). Further, as the motional broadening of the central (m 0) lines is small, an accurate estimate of the residual linewidth W_r (exp) may be obtained from the central region of each experimental spectrum by comparing only this region with a simulated spectrum computed at W_m W_r (exp) constant, i.e. τ 0.

The procedure for determining the best-fit values of ϕ_0, β_0 and τ per spectrum was first to vary ϕ_0 and β_0 (bearing in mind the remarks of the previous section) using an intrinsic linewidth W_r for all the lines (i.e. τ 0), until all the main features of the experimental spectrum showed up. The value of τ was then increased, and small adjustments made in ϕ_0, β_0 and W_r, until the best overall fit was obtained.

For the motional narrowing case one expects a Lorentzian lineshape but inhomogenous broadening due to unresolved proton couplings will make the lines somewhat Gaussian. Both pure Gaussian and Lorentzian lineshapes were tested, but it was found that a superposition of those functions furnished the best fit. This was accomplished by generating normalized Gaussian as well as Lorentzian absorption functions and at each individual orientation (γ and η values) those functions were weighted at a fixed ratio. In Eqns 21 and 23 the proper Γ_r (Gauss) or Γ_r (Lorentz), calculated from W_r, had to be inserted. It was found that the simulated derivative spectra exhibited the best overall fit when a 1 : 1 ratio of the two functions was employed at all temperatures. The spectra were refined by variation of W_r. The final W_r was not constant at all temperatures. From Table I it is seen that W_r is monotonously decreasing from 0.6 to 0.3 mT when raising the temperature. This tendency is in accord with the decreasing contribution of anistropy in any unresolved hyperfine coupling as motion increases. Variation in the residual linewidth has been observed before [4, 8, 13, 15] and treated phenomenologically [4, 8, 15].

The simulated spectra (Fig. 6) were consistently scaled to the same amplitude of the central peak as the corresponding experimental ones. Attempts to scale according to double integrals of derivative spectra were less satisfactory because of uncertainty in the experimental integrals. The total number of parameters would make an automatic iterative procedure somewhat hazardous. Nevertheless, the good agreement between experimental and simulated spectra (except Fig. 6b) based on visual inspection gives us confidence to believe that a consistent set of parameters has been selected. It has to be kept in mind, however, that some of the parameters are interdependent in the sence that they for small variations have similar, but not identical, overall effects on the spectra. This is especially the case for W_r and the Gaussian-Lorentzian lineshape mixture.

Our results show that the introduction of time dependent linewidths is very important and the spectra are dramatically improved. This is examplified in Fig. 7, where spectra have been simulated (with the same double integral), the first including time dependence (full line) and the second neglecting time dependence (dotted line). The different broadenings at various positions of the spectrum are immediately seen. Further, the separation of the high and low field extrema is found to be different from

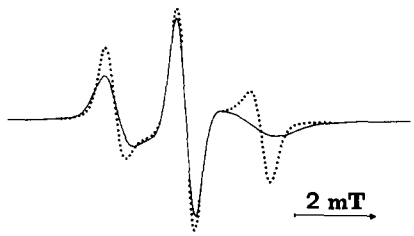

Fig. 7. Demonstration of the effect of the introduction of time dependent linewidth. Full line: Spectrum simulated with the parameter set used in Table I for +10.6 °C (cf. Fig. 6d). Dotted line: Same spectrum where the time dependent effect has been neglected ($\tau = 0$). Both spectra have been normalized to the same double integral.

the theoretical maximum splitting $2T'_{max} = 2\bar{T}_{yy}$ (Eqn 26). The main effect is at the high field region ($m = -1$), whereas the central peak is the part that is affected the least. This finding justifies the amplitude scaling applied in Fig. 6. Mere adjustment of W_r, without applying any dynamic lineshape, never improves the agreement with the experimental spectrum to any appreciable extent. In our earlier work [1] on stearic acid spin labels, $I(m, n)$, we had not yet introduced any time dependence. Preliminary simulations show, as expected, that also in this case agreement with experimental spectra may be obtained with the present model.

As seen from Table I, ϕ_0 increases gradually from 0° to about 90° as the temperature goes from −31 °C to 0 °C. The increase of β_0 is more gradual and probably starts already in this low temperature range, but low values of β_0 have a small effect compared to the effect of ϕ_0 in this region. Hence the failure of the model to include both modes of motion for $\phi_0 < 90°$ is not a serious one. Above 0 °C the angle of wobble, β_0, has to be introduced. It is most easy to fit spectra when $\beta_0 = 0°$ (low temperature) and when $\phi_0 = 90°$ (high temperature) but in the "overlap" region ($\phi_0 \neq 90°$; $\beta_0 \neq 0°$) the spectra are more challenging.

The inferior fit derived for the spectrum at −10 °C (Fig. 6b) was not possible to improve with the present model. The simplest explanation would be that at this temperature there are two phases present, but today we have not further experimental results supporting such a case. Hence, when the correlation times from Table I are plotted as an Arrhenius graph (Fig. 8) there is no obvious indication of an eventual phase transition. Here $\log(1/\tau_{eff})$ is plotted vs. $1/K$, where

$$\left.\begin{aligned} \frac{1}{\tau_{eff}} &= \frac{1}{\tau_a} && \text{for temperatures below 0°C} \\ \frac{1}{\tau_{eff}} &= \frac{1}{\tau_{at}} + \frac{1}{\tau_t} && \text{for temperatures above 0°C} \end{aligned}\right\} \tag{27}$$

As seen, a linear dependence is obtained over the whole temperature range studied. Only an ill defined transition in the region −15 to −5 °C has been reported for egg lecithin so far [16], which we hardly would expect to detect in our experiments. An activation energy of 13.8 kJ · mol^{-1} (3.3 kcal · mol^{-1}) is calculated, a reasonable value for a lipid system. In the literature it is not uncommon to estimate correlation times from applitude or linewidth ratios according to the theory developed for rapid isotropic motion. Even small tendencies to anisotropic motion will invalidate such

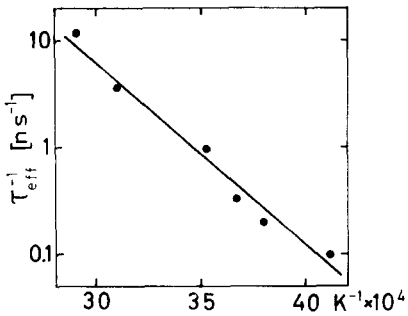

Fig. 8. Arrhenius representation of the temperature behaviour of the simulated correlation times (Table I; Eqn 27) for the 3-doxyl-cholestane spin label in aqueous egg lecithin dispersion.

calculations. This may be examplified by the experiments at the higher temperatures applied in our work for which the motions most closely would approximate the isotropic case; for example τ = 1.8 and 2.7 ns for 71° and 39°, respectively, compared with τ_{eff} = 0.08 and 0.26 ns, applying the present theory that accounts for anisotropic motion.

CONCLUSIONS

The treatment of spin-label motion presented is not generally applicable because of (a) physical limitations of the model, and (b) exclusion of pseudosecular terms in linewidth calculations. But the overall agreement with our experiments is very good, considering that the model involves only two different motional modes and that only four parameters are used (i.e. ϕ_0, β_0, W_r (at fixed line shape), and τ(= τ_{eff})) for the whole temperature range. The computational time for a simulation, including double integral scaling, is modest and requires only about one minute per spectrum. Results show that the present model satisfactorily accounts for the motion of steroid spin label *II* in lecithin bilayer vesicles over a wide temperature range. The model is physically realistic for spin labels in membranes since membrane lipids (and proteins) act as restricting walls, so that the motion of spin labeled molecules fitting into the bilayer may be expected to be rapid but confined within certain angular limits.

The present model should not be suitable for spin labels in isotropic viscous media or solutions, for which a rotational diffusional model will be better. For spin labels in membranes and in many cases for spin labels attached (bound) to proteins and other macromolecules the present model has the great advantage of defining the motion and its limits in a way that is consistent with molecular architecture of the system. For spin labels attached to proteins in solution both rapid restricted rotations and diffusional rotations may together determine the spectral shape. Here it may be best first to calculate $\bar{g}_{xx}$, $\bar{T}_{xx}$ etc. using the present model, and then use these values in a slow rotational diffusion analysis, (employing a different, probably longer, rotational correlation time). It would be interesting to compare our results with motional parameters derived from stochastic theories for anisotropic liquids [3].

ACKNOWLEDGEMENTS

We thank the European Molecular Biology Organization, the Swedish Natural Science Research Council, and the Swedish Medical Research Council for financial support.

REFERENCES

1 Israelachvili, J., Sjösten, J., Eriksson, L. E. G., Ehrström, M., Gräslund, A. and Ehrenberg, A. (1973) Biochim. Biophys. Acta 339, 164–172
2 McCalley, R. C., Shimshick, E. J. and McConnell, H. M. (1972) Chem. Phys. Lett. 13, 115–119
3 Polnaszek, C. F., Bruno, G. V. and Freed, J. H. (1973) J. Chem. Phys. 58, 3185–3199
4 Schindler, H. and Seelig, J. (1973) J. Chem. Phys. 59, 1841–1850
5 Libertini, L. J., Waggoner, A. S., Jost, P. C. and Griffith, O. H. (1969) Proc. Natl. Acad. Sci. U.S. 64, 13–19
6 Jost, P., Libertini, L. J., Herbert, V. C. and Griffith, O. H. (1971) J. Mol. Biol. 59, 77–98
7 McFarland, B. G. and McConnell, H. M. (1971) Proc. Natl. Acad. Sci. U.S. 68, 1274–1278
8 Jost, P. C. and Griffith, O. H. (1973) Arch. Biochem. Biophys. 159, 70–81
9 Lapper, R. D., Paterson, S. J. and Smith, I. C. P. (1973) Can. J. Biochem. 50, 969–981
10 Lefebvre, R. and Maruani, J. (1965) J. Chem. Phys. 42, 1480–1502
11 Wertz, J. E. and Bolton, J. R. (1972) Electron Spin Resonance, Chap. 9, McGraw-Hill, New York
12 Fraenkel, G. K. (1967) J. Phys. Chem. 71, 139–171
13 Wilson, R. and Kivelson, D. (1966) J. Chem. Phys. 44, 154–168
14 Hubbell, W. L. and McConnell, H. M. (1969) Proc. Natl. Acad. Sci. U.S. 64, 20–27
15 Goldman, S. A., Bruno, G. V., Polnaszek, C. F. and Freed, J. H. (1972) J. Chem. Phys. 56, 716–735
16 Ladbrooke, B. D. and Chapman, D. (1969) Chem. Phys. Lipids 3, 304–367
17 Michon, P. and Rassat, A. (1974) J. Org. Chem. 39, 2121–2124